Measurement of Charge Exchange between H_2 and Low-Energy Ions with Charge States $35 \leq q \leq 80$

B. R. Beck,[1] J. Steiger,[1] G. Weinberg,[2] D. A. Church,[2] J. McDonald,[1] and D. Schneider[1]
[1]*Lawrence Livermore National Laboratory, Livermore, California 94550*
[2]*Physics Department, Texas A&M University, College Station, Texas 77843-4242*
(Received 10 January 1996)

Charge-exchange cross sections for collisions between H_2 and ions with unusually low center-of-mass energies ($\approx$6 eV) and high-charge states (Xe^{q+}:$35, 43 \leq q \leq 46$, Th^{q+}:$73 \leq q \leq 80$) have been measured using a Penning ion trap. A nondestructive measurement technique permitted both primary and product ion analysis. The data, averaged over the charge states indicated above, are consistent with a total cross section that scales linearly with ion charge q. The true double-capture cross section is found to be about 25% of the total cross section at high q. The results are compared to predictions of the absorbing-sphere model. [S0031-9007(96)00972-6]

PACS numbers: 34.70.+e

Charge exchange between H_2 and highly charged ions of Xe (Xe^{35+}, Xe^{43+} to Xe^{46+}) and Th ($Th^{73+}$to Th^{80+}) has been studied at unusually low center-of-mass energies for such high-charge states. This energy is calculated to be about 6 eV. Total electron-capture cross sections in this energy range have been predicted using the absorbing-sphere model [1], that is based on the Landau-Zener theory. This model is expected to be most valid for high charge, and predicts a cross section that scales slightly less than linearly with charge state q. On the other hand, the cross section for double-electron capture versus q is not well estimated, and is a matter of continuing investigation [2–4]. The present measurements, averaged over the charge states indicated above, are consistent with a total cross section that scales linearly with q to $q = 80+$. The true double-capture cross sections at intermediate q (44+) and high q (80+) are about 25% of the total cross sections. True double capture occurs when both electrons remain on the ion [5].

The present measurements were performed at Lawrence Livermore National Laboratory (LLNL), using the LLNL Electron Beam Ion Trap (EBIT) [6] and RETRAP systems [7]. The highly charged ions were produced in EBIT, extracted, analyzed, and transported to the cryogenic Penning trap of RETRAP, where the charge-exchange measurements were performed. The time evolution of the numbers of ions in sequential charge states was determined using a nondestructive technique, and the data were fitted to rate equations to determine the charge-exchange rates. From the rates, the ratio of the true double-capture cross section to total cross section was obtained without further analysis. However, a determination of an absolute cross section requires knowledge of ion velocities and the density of H_2. The ion velocities were determined from ion signals and storage properties, and the density of H_2 was determined from measurements performed on Ar^{11+}, for which the electron-capture cross section had previously been measured [8].

Trapped highly charged high-Z ions (HCHZI) with low energies are currently being studied in x-ray and beam sources like EBIT, and in ion traps. Often in these studies the subject under investigation is a specific ionization state of a highly charged ion, as in mass-spectrometry measurements [9]. Typically, the main loss of an ion in a specific ionization state is via charge exchange; hence, an understanding of charge-exchange processes in ion sources and in mass-spectrometry measurements is important. Although the combination of HCHZIs with low energies is rare in nature, it may be encountered in planned fusion-energy devices such as the International Thermonuclear Experimental Reactor (ITER) and in certain astrophysical events. In addition, when multiple electrons are captured into high-n states, the decay may be by photon emission, or by autoionization. This affects the ratio of, for example, the true double-capture cross section to the total cross section, and also the "inverted" populations interesting for x-ray laser schemes.

Charge-exchange processes of multiply charged ions have previously been studied in crossed [2–4,10] and merged [11] beam arrangements, as well as in traps [12]. However, there remains a paucity of data at the lowest energies, combined with high-charge states, which the present measurements begin to address.

The cryogenic Penning trap employed is schematically shown in Fig. 1, and was modeled after the open-ended cylindrical Penning trap developed by Gabrielse *et al.* [13]. This trap is composed of five cylindrical electrodes (two end, two compensation, and one ring). This design creates a harmonic axial potential well in the central region of the trap when the end, compensation, and ring electrode potentials are V_0, $0.118V_0$, and 0, respectively. Radial confinement was provided by a 4 T uniform magnetic field that was collinear with the axis of the electrodes.

The highly charged ions from EBIT were quickly released following production, yielding an ion beam with a pulse width of about 20 μs and a kinetic energy of

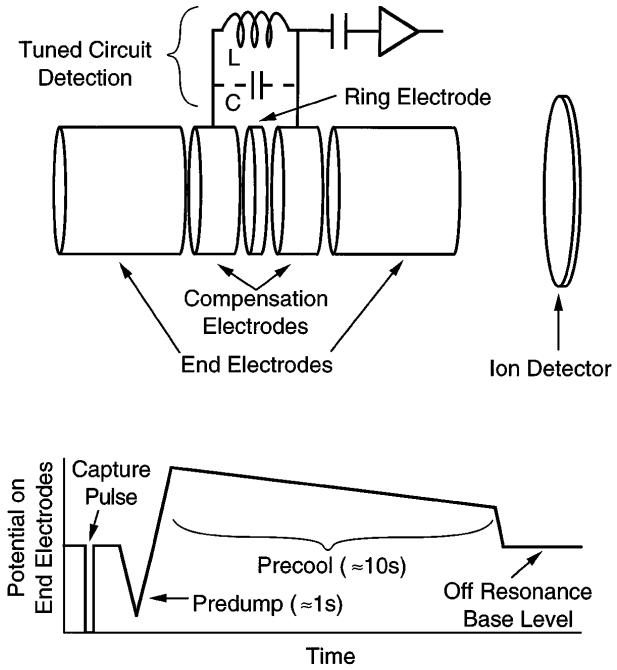

FIG. 1. Schematic of open-ended cylinder trap and detection circuit, and timing of end-electrode voltages. The capture was applied only to the left electrode (i.e., capture end electrode), whereas, the "predump" (used to remove hot ions) and "precool" (used to cool the remaining ions) waveforms were applied to both end electrodes.

about $q \times 4.5$ keV. Since only a single charge state was desired, the extracted ions were directed through an analyzing magnet. Next, the ions were decelerated upon entering a long cylindrical electrode situated above the Penning trap, which was pulsed in potential from near the EBIT extraction potential to near ground at the appropriate time. As the decelerated ions entered the Penning trap, the capture end electrode (see Fig. 1) was quickly switched from ground to V_0 (about 70 V), which trapped the ions. Only a few ions (up to about 30) were captured per pulse, since many of the ions were lost or rejected in the extraction, magnetic analysis, deceleration, and capture phases.

The two compensation electrodes were connected by a 770 μH inductor which, in conjunction with trap capacitance, produced a parallel tuned circuit (see Fig. 1). This circuit had a quality factor Q near 250, and a resonant frequency $\nu_0 = 1.21$ MHz. A cryogenic low-noise preamplifier was attached to this circuit, allowing the rf voltage across it to be monitored. For an ion oscillating axially in the trap, a current I_Z existed in the tuned circuit which produced a voltage $V_Z = I_Z R$, when the axial frequency of the ion was on resonance with the tuned circuit that had parallel resistance R. Since the ion signal was proportional to the impedance, which was small except for frequencies near resonance, only ions near resonance were detected.

An ion with low axial energy oscillated axially in the trap with angular frequency

$$\omega_z = 2\pi\nu_z = \sqrt{\frac{qeV_0C_2}{md^2}}. \qquad (1)$$

Here qe and m are the charge and mass of the ion, respectively. For the present trap $C_2 = 0.5449$ and $d = 0.512$ cm. As an example, for $^{136}Xe^{44+}$, the condition $\nu_z = \nu_0$ occurred when $V_0 = 89.6$ V, as can be seen from Figs. 2(a) and 2(b). For N ions with the same q and m, oscillating incoherently at resonance, the mean squared current induced was

$$\langle I^2_{\text{total}}\rangle = \sum_i^N \langle I_z^2(i)\rangle = \frac{N\langle E_z\rangle}{T_z R}. \qquad (2)$$

Here, $\langle\ \rangle$ means a time average over an ion axial oscillation time $2\pi/\omega_z$, $I_z(i)$ was the current induced by the ith ion, $\langle E_z\rangle$ was the average axial kinetic energy per ion, and $T_z = 4\,md^2/(qe)^2\gamma^2 R$ was the time constant for damping the axial energy of ions on resonance, due to energy dissipation in R. The coupling constant γ for the compensation electrodes was 0.9 [13]. The input to the preamplifier V_p was an incoherent combination of the on-resonant ion signals and the noise of the circuit and preamplifier input V_n, added in quadrature:

$$V_p^2 = \langle I^2_{\text{total}}\rangle R^2 + V_n^2 = \frac{N\langle E_z\rangle R}{T_z} + V_n^2. \qquad (3)$$

To increase the signal-to-noise ratio, the preamplifier output was filtered with a spectrum analyzer that was set to record a narrow frequency bandwidth, $\Delta f \approx 9$ kHz, around the tuned-circuit resonance frequency. Figure 2 shows the spectrum-analyzer signal and the corresponding ramp of the potential V_0 as a function of time [the signals in Figs. 2(b) and 2(c) are proportional to V_p^2]. For the data in this figure, the ions were held in the Penning trap for 200 s. During this time, V_0 was ramped as shown in Fig. 2(a) every 10 s, and the spectrum-analyzer signal was recorded (called a scan) for each ramp. Figure 2(b) shows the first scan started 2 s after the ions were captured, and Fig. 2(c) shows the 11th scan started 102 s after the ions were captured. After the 200 s hold time, the ions were released from the trap. The process of capturing, measuring, and releasing the ions (called a cycle) was repeated, and the data averaged to further improve the signal-to-noise ratio. The data shown in Figs. 2(b) and 2(c) are the average of 50 cycles. Ions that reside in the harmonic region of the trap are desired to minimize the signal linewidths. The highest-energy trapped ions were removed at the beginning of each cycle by adiabatically lowering the end-electrode potential from V_0 to about $V_0/6$ (see "predump" in Fig. 1). For some measurements, the remaining ions were then slowly swept through resonance with the tuned circuit (see "precool" in Fig. 1) to lower their axial energy.

Figure 2(b) shows that the injected ions were all Xe^{44+} in that measurement. As storage time increased, the Xe^{44+} signal decreased, and the signals for lower-charge states first increased and then decreased with time. The evolution of the number of ions in each charge state can be modeled as

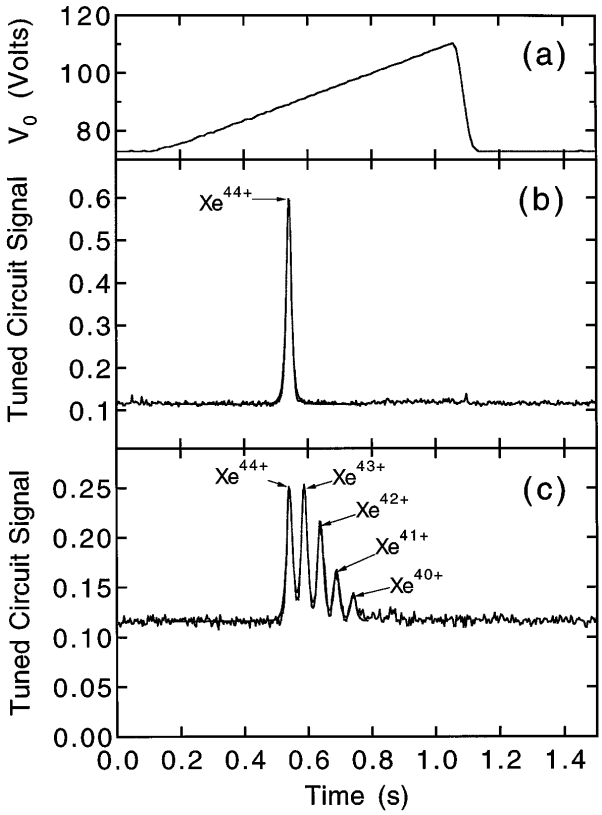

FIG. 2. (a) Ramp of V_0 versus time, and the corresponding spectrum-analyzer signals [proportional to V_p^2, see Eq. (4)] started 2 s (b) and 102 s (c) after the ions were captured. The area of a peak is related to the number of ions in that charge state.

$$dN_q/dt = -\gamma_q N_q \tag{4a}$$

$$dN_{q-1}/dt = -\gamma_{q-1} N_{q-1} + \gamma_q^s N_q \tag{4b}$$

$$dN_x/dt = -\gamma_x N_x + \gamma_{x+1}^s N_{x+1} + \gamma_{x+2}^d N_{x+2}, \tag{4c}$$

for $x = q - 2, q - 3, \ldots$. Here q is the charge of the primary ion, N_x is the number of ions with charge x, and γ_x^s, γ_x^d, and $\gamma_x = \gamma_x^s + \gamma_x^d$ are the single-, double-, and total-charge-exchange rates for ions with charge x. The data were fitted by the solutions of Eq. (4). The single-, double-, and total-charge-exchange rates were obtained with the assumption that the charge-exchange rates are proportional to charge [i.e., $\gamma_{q-1}^s = (q - 1/q)\gamma_q^s$], consistent with the overall results and theory. Note, the fits are typically over the highest 3 or 4 successive charge states; hence, this assumption does not significantly change the results.

Figure 3 shows the measured ion number and the fitted curves versus time for a primary ion of Xe^{44+}. The measured ion numbers were obtained from scans similar to those shown in Fig. 2 by fitting the peaks in each scan to obtain the areas under each peak [close inspection of Fig. 2(c) will reveal the fitted line]. Note that this is only a relative measurement of the number of ions. The areas were then scaled to account for several effects associated with the measurement. (a) During the ramping phase shown in Fig. 2(a), an ion's axial energy is changed

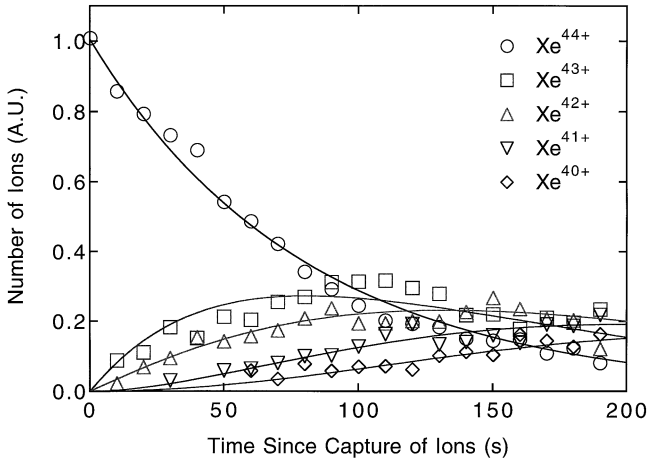

FIG. 3. Time dependence of ion number for five ion-charge states. The points are data and lines are fits to the solutions of Eq. (4).

adiabatically, thus E_z is changed in such a way that E_z/ω_z is constant. The higher an ion's charge, the less ramping and hence compressional heating required to bring it on resonance with the tuned circuit, as can be seen in Fig. 2. It can be shown that an ion's on-resonance energy scales as $q^{-1/2}$ as compared to the energy it has during the longer, nonramp phase. From Eqs. (2) and (3) it follows that the signal is proportional to $q^2\langle E_z\rangle$, hence, the data were scaled by $q^{-3/2}$. (b) An ion on tuned-circuit resonance loses energy at the rate $-E_z/T_z$ (we have calculated T_z from the trap parameters and found it to be close to the measured value). Although this loss was confined to the short times that the ions spend on resonance during the ramps, the cumulative effect over a cycle was not negligible, and required an adjustment. (c) The measured signals were proportional to the average axial energy and not the average total energy of the ions. It was necessary to account for the mixing of axial and radial energies that occurred over the long time of the cycle. Therefore, the areas were scaled by $q^{-3/2}\exp(-\alpha t)(1 + A\exp[-\beta t])$, where α is the energy damping rate from (b), and A and β are parameters that allow for mixing of axial and radial energy. A is a simple function of the initial ratio of $\langle E_z\rangle/\langle E_\perp\rangle$, thus allowing us to determine $\langle E_\perp\rangle$ from $\langle E_z\rangle$. Some of the data could be analyzed by a method independent of ion energy [14], in fact, independent of items (a), (b), and (c) above. The results of this latter analysis confirmed the efficacy of the corrections discussed above. However, we choose to present the former analysis because it could be used for all the data and it yields the ratio $\langle E_z\rangle/\langle E_\perp\rangle$.

The fitted rates are given by $\gamma_x = n\langle\sigma_x v\rangle$, where n is the number density of the H_2 target. Observed [8] cross sections σ_x are, to good approximation, velocity independent in the energy range of our data. The mean-squared velocity of the ions was obtained from an analysis of ion signals and the calculated storage properties of the trap. Ions that resided in the harmonic region of the trap must have had an energy less than about $q \times 12$ eV

[15]. We adjusted the predump voltage (see Fig. 1) until the ion signals indicated, from the width of the signal, that all ions remaining after the predump phase are in the harmonic region of the trap. Hence, we use $\gamma_x \cong n\sigma_x\langle v^2\rangle^{1/2}$ to obtain the cross sections from the fitted rates. A measurement of γ_{11} for Ar^{11+} together with the published value for σ_{11} [8] enabled a determination of the H_2 density. With conditions similar to that described above, but with only Be ions initially trapped, we used a time of flight measurement and observed only Be ions and hydrogen product ions. This indicated good H_2 target gas purity in the cryogenic vacuum.

The absorbing-sphere model predicts a total cross section that varies nearly linear with q as shown by the dot-dashed line in Fig. 4(a). In the calculation, the Franck-Condon factor for H_2 was chosen as 0.1, in accord with earlier work [1], and a correction to account for the polarization of H_2 by the high charges was included [16]. The data in Fig. 4 are plotted in a simplified way by averaging the measurements for 10% ranges of charge states (i.e., Xe^{43+} to Xe^{46+} and Th^{73+} to Th^{80+}), since variations with charge in these ranges are not significant relative to the measurement uncertainties. The data lie well above the theory, especially at high q, although it should be noted that the normalizing Ar^{11+} cross section also lies above the calculation. Our present data would be consistent with the theory if this were not the case.

The ratios of the true double-capture cross section to the total cross section are plotted versus q in Fig. 4(b). This ratio agrees with the published result for Ar^{11+}, and rises with q. This is consistent with the expectation that double capture preferentially occurs into radiatively stabilized states for high q. There is no apparent increase of the mean values for $q \geq 35+$, indicating that transfer ionization, in which one captured electron is lost during the collision or through an Auger process, may be minimal. Transfer ionization is theoretically largest at low q, and contributes to the single-capture fraction in the present measurements.

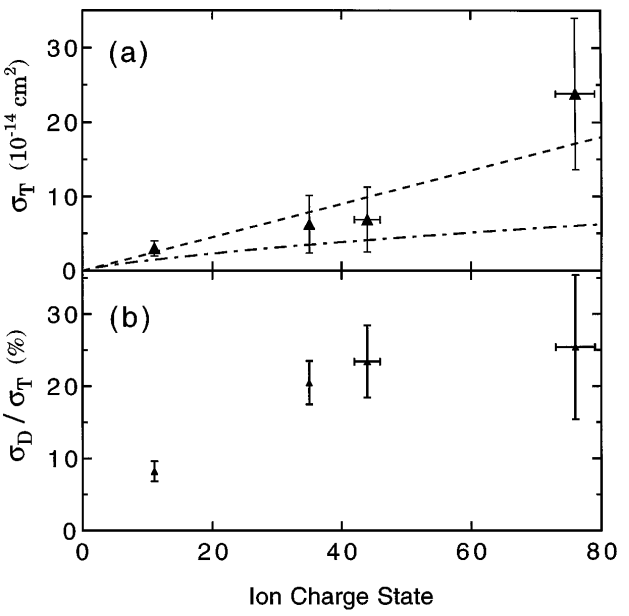

FIG. 4. Plots of (a) the total cross section and (b) the ratio of true double-capture cross section to total cross section for different highly charged ions as a function of ion-charge state q. The dashed line is a linear fit to the data, and the dot-dashed line is a plot of the absorbing-sphere model.

In summary, low-energy charge-exchange has been studied for high-charge states using a specialized ion production and storage apparatus (RETRAP). The measured total cross sections are consistent with a linear dependence on charge. The ratio of the true double-capture cross section to the total cross section is found to be independent of q to within experimental uncertainties for $q \geq 35$, and is about 25%.

We wish to express our thanks to Ed Magee and Dan Nelson for their help in the development and setup of the RETRAP system. This work was performed under the auspices of the U.S. Department of Energy by the Lawrence Livermore National Laboratory under Contract W-7405-ENG-48.

[1] R. E. Olson and A. Salop, Phys. Rev. A **14**, 579 (1976).
[2] H. Cederquist, H. Andersson, G. Astner, P. Hvelplund, and J. O. P. Pedersen, Phys. Rev. Lett. **62**, 1465 (1989).
[3] H. Cederquist, H. Andersson, E. Beebe, C. Biedermann, L. Broström, Å. Engström, H. Gao, R. Hutton, J. C. Levin, L. Liljeby, M. Pajek, T. Quinteros, N. Selberg, and P. Sigray, Phys. Rev. A **46**, 2592 (1992).
[4] H. Cederquist, C. Biedermann, N. Selberg, and P. Hvelplund, Phys. Rev. A **51**, 2191 (1995).
[5] If an ion captures two electrons from a H_2 molecule, then one electron may be ejected through autoionization, which results in one net electron captured by the ion. When both electrons radiatively stabilize, it is called true double capture.
[6] R. E. Marrs, M. A. Levine, D. A. Knapp, and J. R. Henderson, Phys. Rev. Lett. **60**, 1715 (1988).
[7] D. Schneider, D. A. Church, G. Weinberg, J. Steiger, B. Beck, J. McDonald, E. Magee, and D. Knapp, Rev. Sci. Instrum. **65**, 3472 (1994).
[8] S. Kravis, H. Saitoh, K. Okuno, K. Soejima, M. Kimura, I. Shimamura, Y. Awaya, Y. Kaneko, M. Oura, and N. Shimakura, Phys. Rev. A **52**, 1206 (1995).
[9] C. Carlberg, H. Borgenstrand, G. Rouleau, R. Schuch, F. Söderberg, I. Bergström, R. Jertz, T. Schwarz, J. Stein, G. Bollen, H.-J. Kluge, and R. Mann, Physica Scripta **T59**, 196 (1995).
[10] R. Mann, F. Folkman, and H. F. Beyer, J. Phys. B **14**, 1161 (1981).
[11] M. S. Huq, C. C. Havener, and R. A. Phaneuf, Phys. Rev. A **40**, 1811 (1989).
[12] D. A. Church, Phys. Rep. **228**, 254 (1993).
[13] G. Gabrielse, L. Haarsma, and S. L. Rolston, Int. J. Mass Spectrom. Ion Processes **88**, 319 (1989).
[14] J. Steiger, D. A. Church, G. Weinberg, B. R. Beck, J. McDonald, and D. Schneider (to be published).
[15] A center of mass calculation with the target gas at rest yields a center-of-mass energy of 6 eV.
[16] R. Olson, private communication to D. A. C. (1995).